Journal of Microbiological Methods 189 (2021) 106302

Contents lists available at ScienceDirect

Journal of Microbiological Methods

journal homepage: www.elsevier.com/locate/jmicmeth

An adaptable and non-invasive method for tracking *Bifidobacterium animalis* subspecies *lactis* 420 in the mouse gut

Marissa A. Lopez-Pier [b,c], Matthew P. Koppinger [b,f], Preston R. Harris [b,f], Danielle K. Cannon [a,b], Rinku S. Skaria [a,b], Bonnie L. Hurwitz [g], George Watts [g], Shravan Aras [h], Marvin J. Slepian [b,c,g,i], John P. Konhilas [a,b,c,d,e,f,*]

[a] *Department of Physiology, University of Arizona, Tucson, AZ, USA*
[b] *Sarver Molecular Cardiovascular Research Program, University of Arizona, Tucson, AZ, USA*
[c] *Department of Biomedical Engineering, University of Arizona, Tucson, AZ, USA*
[d] *Department of Molecular and Cellular Biology, University of Arizona, Tucson, AZ, USA*
[e] *Department of Cellular and Molecular Medicine, University of Arizona, Tucson, AZ, USA*
[f] *Department of Nutritional Sciences, University of Arizona, Tucson, AZ, USA*
[g] *Bio5 Institute, University of Arizona, Tucson, AZ, USA*
[h] *Menolabs, LLC, Tucson, AZ, USA*
[i] *Department of Medicine, University of Arizona, Tucson, AZ, USA*

ARTICLE INFO

Keywords:
Bifidobacterium animalis lactis subspecies 420
Translocation
Indocyanine green
ISOVUE-300
Quantitative PCR

ABSTRACT

Probiotic strains from the *Bifidobacterium* or *Lactobacillus* genera improve health outcomes in models of metabolic and cardiovascular disease. Yet, underlying mechanisms governing these improved health outcomes are rooted in the interaction of gut microbiota, intestinal interface, and probiotic strain. Central to defining the underlying mechanisms governing these improved health outcomes is the development of adaptable and non-invasive tools to study probiotic localization and colonization within the host gut microbiome. The objective of this study was to test labeling and tracking efficacy of *Bifidobacterium animalis* subspecies *lactis* 420 (B420) using a common clinical imaging agent, indocyanine green (ICG). ICG was an effective *in situ* labeling agent visualized in either intact mouse or excised gastrointestinal (GI) tract at different time intervals. Quantitative PCR was used to validate ICG visualization of B420, which also demonstrated that B420 transit time matched normal murine GI motility (~8 hours). Contrary to previous thoughts, B420 did not colonize any region of the GI tract whether following a single bolus or daily administration for up to 10 days. We conclude that ICG may provide a useful tool to visualize and track probiotic species such as B420 without implementing complex molecular and genetic tools. Proof-of-concept studies indicate that B420 did not colonize and establish residency align the murine GI tract.

1. Introduction

The gut microbiome is a large and diverse community of microorganisms that inhabit and interact with the human intestinal lining (Putaala et al., 2010). The unique biological relationship between gut microbiota and its host is termed symbiosis under healthy conditions. This symbiotic relationship is preserved by a mucosal layer containing both antimicrobial peptides and innate lymphoid cells. Disruption of symbiosis, or *dysbiosis*, can instigate detrimental interactions between colonic microbiota, their metabolites, and the host immune system activating the innate immune system and instigating a pro-inflammatory response (Brown et al., 2013). Dysbiosis of the microbiome is associated with several metabolic disorders including obesity, diabetes, and cardiovascular disease (Karlsson et al., 2013). Many studies demonstrate that host-microbiota symbiosis is maintained by microbiota and microbiota-derived metabolites in gut, which lay in close proximity to immune-directing tissue (Bauer, 2018a; Bauer et al., 2018b; Zadeh-Tahmasebi et al., 2016). These microbiota-derived factors impact metabolic processes including nutrient sensing and whole-body glucose regulation. For instance, the gut shows high expression of

* Corresponding author at: Univ. of Arizona, Dept. of Physiology, Biomedical Engineering, Molecular and Cellular Biology, Cellular and Molecular Medicine, Nutritional Sciences, Sarver Molecular Cardiovascular Research Program, 1656 E Mabel St, Tucson, AZ 85724, USA.
E-mail address: konhilas@email.arizona.edu (J.P. Konhilas).

https://doi.org/10.1016/j.mimet.2021.106302
Received 20 April 2021; Received in revised form 7 August 2021; Accepted 9 August 2021
Available online 13 August 2021

bacterial-derived transcripts for carbohydrate metabolism, suggesting a central role in this process (Zoetendal et al., 2012).

The mechanism underlying the impact of dysbiosis on disease is not well understood in part due to the complexity of the gut microbiota and the gut environment (Mowat and Agace, 2014; Tremaroli and Bäckhed, 2012). In humans, the gastrointestinal (GI) tract stretches over 20 m with an intestinal surface area 100 times greater than body surface area (DeSesso and Jacobson, 2001). Additionally, the GI tract is home to several unique habitats. Due to changing physiological needs, portions of the small and large intestines differ significantly in pH, bile acid concentration, and oxygen content (Donaldson et al., 2015). These conditions, along with available fuel sources, determine the amount and type of bacteria that can survive in a given section of the GI tract (Derrien et al., 2010; Stearns et al., 2011). Given this, certain probiotic strains may be preferentially equipped to survive and act in certain sections of the GI tract.

Probiotics are defined by the World Health Organization as "live microorganisms that confer a health benefit to the host when consumed in adequate amounts (Sanders, 2011)." A common probiotic strain is *Bifidobacterium*, a highly diverse gram-positive bacteria from the phylum Actinobacteria and *Bifidobacterium* genus found in oral cavities, GI tracts and dairy products (Fang and Gough, 2013; Lee and O'Sullivan, 2010; Milani et al., 2013; WOESE et al., 1977). Previous work demonstrates that *Bifidobacterium animalis* subspecies *lactis* 420 (B420) positively impacts metabolic syndrome by limiting weight gain, improving glucose metabolism, and reducing low-grade inflammation (Hotamisligil, 2017; Putaala et al., 2008; Stenman et al., 2014a, 2016). In our studies, pre-administration of B420 following a myocardial infarction (MI), a known inflammatory disease, attenuated cardiac damage (Danilo et al., 2017). To better elucidate the mechanisms of probiotics, specifically B420, we must consider not only *how* but also *where* probiotics elicit their actions. Probiotic colonization, localization, and residence in the GI tract have important implications for determining mechanism of host-microbe interaction. Understanding these basic mechanisms will impact characteristics such as dose, frequency, and length of probiotic administration, critical factors when utilizing B420 and other probiotic strains for therapeutic use.

Probiotic transit, adherence and colonization in both small and large intestines are understudied areas; previous research largely focused on detecting probiotic species in feces and large intestine. Visualization through fluorescence is challenging or not possible due to poor genetic accessibility and lack of vector systems for Bifidobacterial genomes (Dominguez and O'Sullivan, 2013; Grimm et al., 2014; Lee and O'Sullivan, 2010; Wiles et al., 2006). Therefore, the central goal of this proof-of-concept study was to develop an efficient, cost-effective technique to visualize and track probiotic transit through the GI tract in as little as a single digestive cycle in a mouse.

We hypothesized that labeling of microbial species with an externally detectable marker would allow detection as to their specific geographic residence/location during transit through the gut. First, we incubated B420 with common, FDA-approved contrast agents, ISOVUE-300 or indocyanine green (ICG), and visualized by x-ray fluoroscopy (ISOVUE-300) or fluorescence (ICG) along the GI tract at different timepoints. Further, we validated and quantified B420 using quantitative PCR at different regions of the GI tract. We found that ICG was a more effective labeling agent over ISOVUE-300, and following a single bolus of B420, we also demonstrated B420 transit time matched normal murine gut motility of approximately 8 h. Importantly, we demonstrated that B420 did not colonize the host gut microbiome, even following 10 consecutive days of B420 administration, where the amount of detectable B420 diminished to control levels within 24–48 h.

2. Materials & methods

2.1. Incubation of B420 with ICG

A determination of B420 stability and B420 growth curve was executed using purified stock of B420 (see Supplemental Data, Fig. S1). A serial dilution of 1 mg/ml solution (the solubility concentration of ICG in water) from 1 mg/ml to 0.001 mg/ml, was plated in a 96 well plate and imaged to optimize the ICG fluorescent signal. Based on this, 0.01 mg/ml was used to label 12-h cultured bacteria for 1 h in dark conditions. The pellets were then centrifuged at 16,000 x*g* and washed three times in sterile saline. The dilutions were imaged to confirm labeling had occurred. Both labeled pellets and ICG alone (0.01 mg/ml) were administered to C5Bl/6 J mice. The signal was tracked over an 8-h period. The intestinal tract was excised from the animal and imaged with the same parameters as the 96 well plate. To determine the stability of B420-labeled ICG signal, B420 was incubated in dark conditions at 27 °C for a 24-h period with 0.01 mg/ml ICG, pelleted and then re-suspended in culture media free of ICG. Starting at baseline, aliquots were removed every 2 h over a 24-h period, pelleted (while also saving the pellet's initial 1 ml supernatant), and washed for fluorescent imaging.

2.2. Imaging of ICG

The fluorescent imaging was acquired on the Spectral Instruments Imaging LagoX and AMIVIEW software (https://spectralinvivo.com/). A serial dilution of ICG was loaded (200 uL per sample) into a clear 96 well plate. The plate was exposed to a 710 nm excitation and 830 nm emission near infrared (NIR) light within NIR range (800–2500 nm) for 50 s. Sample container, saline, food and intestinal tissue were imaged to control for auto fluorescence with and without ICG. For *in situ* mouse ICG imaging, mice were intubated and ventilated with 0.5–2.0% isoflurane (Phoenix Pharmaceuticals, Inc). Fluorescence was quantified and expressed as photon flux (photons/s) per pixel using standardized AMIVIEW software tools. Fluorescence of ICG alone and ICG labeled B420 bacteria were normalized to the respective control tissue and ICG negative control (gavaged ICG alone), as well as the pixel count in the region of interest (ROI).

2.3. Animals, diet and probiotic administration

All experiments were performed using protocols adherent to guidelines approved by the Institutional Animal Care and Use Committee (IACUC) at the University of Arizona and to 2018 NIH guidelines for care and use of laboratory animals. 12-week-old wild-type male mice (C5Bl/6J; Jackson Laboratories, stock 000664, Bar Harbor, ME, USA) were fed a normal rodent chow (NIH-31:18% fat, 59% carbohydrates, 23% protein; Research Diets, Inc., New Brunswick, NJ, USA) during the study. Mice were randomized into six groups and fed 500ul of the following: B420 incubated in indocyanine green (ICG) (Cardiogreen; Sigma,I2633), ICG at 0.01 mg/ml dilution in saline, B420 incubated in ISOVUE-300 (0%, 40%, 50%) (ISOVUE-300; Bracco Diagnostics), or saline (Fig. 1). B420 was administered by gavage 10^9 colony forming unit (CFU)/500uL saline of *Bifidobacterium animalis* subspecies *lactis* 420 (DuPont Nutrition &Health, Kantvik, Finland; ATCC:SD6685). Following a single administration, mice were randomized to four timepoints: 15 min, 2 h, 4 h, and 8 h for sacrifice, and GI tracts were excised as described in *Tissue Resection*. A separate group of mice was administered B420 at (10^9 CFU/500ul) for 10 consecutive days. Again following randomization, intestinal tracts were excised at either 15 min, 24 h, 48 h, and 144 h (six days) from the final administration as described in *Tissue Resection*.

2.4. Tissue resection and GI tract content scrape

After mice sacrifice, the GI tract was excised from the base of the

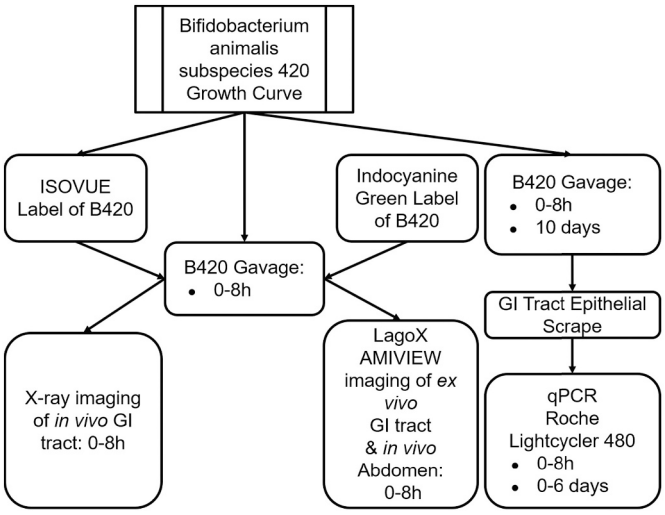

Fig. 1. Experimental workflow and applications used to visualize and track B420. B420 was incubated with contrast agents, ISOVUE −300 or Indocyanine Green (ICG). After washing the B420 pellet post-incubation, the labeled B420 was resuspended and imaged or administered by gavage to male mice. The gastrointestinal (GI) tract was excised and visualized by x-ray imaging (ISOVUE-300) or (bio) flourescent imaging (ICG). Additionally, unlabeled B420 was scraped from the GI tract, and genomic DNA was extracted for qPCR. (For interpretation of the references to colour in this figure legend, the reader is referred to the web version of this article.)

esophagus to the anus and fully extended on an ice-cold stainless steel 8 × 11″ plate covered in saline soaked filter paper. The GI tract was bathed repeatedly with cold saline solution and cut into six sections (duodenum, jejunum, ileum, caecum, proximal colon, and distal colon) based on anatomical landmarks and coloration of the intestinal contents. A sagittal cut exposed the interior of the gut, which was rinsed with saline to remove large, non-adherent debris. Next, an uncharged, standard microscope slide was gently dragged across the exposed interior to extract the epithelial layer and digesta. Samples were flash frozen in liquid nitrogen for storage at −80 °C.

2.5. Semi-quantitative and quantitative PCR

Genomic DNA (gDNA) from bacteria, isolated from the epithelial scrape using a DNA extraction method designed for digesta and fecal samples, was used for end-point PCR (Yu and Morrison, 2004). For semi-quantitative PCR, PCR was performed using AccuPower Premix Mastermix (Bioneer; K-2016) and a 5333 gradient Mastercycler thermocycler (Eppendorf; Hamburg, DE) using primer-specific amplification protocols. B420 PCR protocol was programmed as follows: 3 min at 95C for 1nitial denaturation (1×); 30 s (s) at 95C, 30s at 57C, 1 min at 72C (36×); 5 mins at 72C for final extension; stand at 4C. The 16S PCR protocol was programmed as follows: 2 min at 95C for initial denaturation (1×); 20s at 95C, 30s at 68C, 1 min at 68C (36×); 5 min at 72C for final extension (1×); stand at 4C. Two internal controls were used: (1) gDNA extracted from purified B420 and (2) the variable region 3 (V3) of the 16 s rRNA gene (see Supplemental Table S1 for target sequences) (Sundquist et al., 2007). PCR products were visualized on 1% Agarose gels containing GelRed (Phenix Research Products; RGB-4103). PCR products were imaged in a GBox XT4 (SynGene; Chemiluminescence and Fluorescence Imaging System) and analyzed using IMAGEJ (NIH). Quantitative PCR was performed using SYBR Green qPCR Master Mix (Roche Diagnostics; 04707516001) and Light Cycler 480 (Roche Diagnostics).

2.6. Data analysis

B420 growth curves were fit to an asymmetrical, five-parameter logistic equation (Fig. S1) (Giraldo et al., 2002; Gottschalk and Dunn, 2005). Standard curves were generated from the B420 gDNA extracted from freeze-dried, purified B420 and fit using commercially available LightCycler 480 software (V 1.5). Using the standard curve, gDNA was converted to nanogram (ng) amounts. Cp values were calculated as the absolute value of the turning point which corresponds to the first maximum of the second derivative of the fluorescence sigmoidal curve of the Sybr green in the qPCR reactions. The percent weight gain was determined by subtracting weekly body weight values from starting body weight and expressing as a percentage of starting body weight. The Area Under the Curve (AUC) for body weight was calculated weekly using the trapezoidal method. The differences between AUC and infarct size between mice administered with B420 or saline were analyzed with a two-way ANOVA followed by a Bonferroni post-hoc test; $p < 0.05$ was considered as significant. Results are presented as mean ± standard error of the mean (SEM).

3. Results

3.1. Visualization of ICG-labeled B420

B420 incubated with ISOVUE was detectable by x-ray fluoroscopy *ex vivo*. However, the ISOVUE-300 signal was not sensitive enough to track B420 *in vivo* (see Supplemental data, Fig. S2). Therefore, we moved to another FDA-approved agent, ICG, a contrast agent regularly used to visualize arteries and microvasculature in the brain and skin (Alander et al., 2012). In the following series of *in vitro* experiments, we wished to determine the toxicity of ICG to B420 growth and proliferation while identifying the optimal amount of ICG required for visualization *in vivo*. ICG has known toxicity *in vitro* and *in vivo* (Gale et al., 2004; Grisanti et al., 2004). Previous work demonstrates low cytotoxicity at a clinically relevant concentration of ICG (0.5 mg/ml) (Gale et al., 2004). Accordingly, B420 was cultured in 0.5 mg/ml ICG over a 24-h period to determine B420 toxicity of ICG. We first determined the dynamic range of excitation-emission for ICG fluorescence (see Methods). As evidenced in the control (Fig. 2A; ICG alone), 0.002 mg/ml ICG was the peak signal that became saturated at higher concentrations. Similar to the ISOVUE-300 incubation protocol, we incubated B420 in culture media containing a range of ICG concentrations (0.001-1 mg/ml) and determined the optimal ICG concentration for B420 staining and visualization by fluorescence. When B420 was incubated with ICG (Fig. 2B), the peak signal was 2.5-fold less than ICG alone and occurred at a concentration of 0.01 mg/ml ICG with little difference in fluorescence at 0.002 mg/ml (3.9-fold) or 0.001 mg/ml (2.7-fold) ICG culture. As evidenced from the growth curve (Fig. 2C), the ICG-B420 culture showed a longer lag phase, demonstrating mild cytotoxicity. To determine the persistence or decay of labeled ICG-B420 fluorescence during B420 proliferation in culture, we imaged bacterial pellets every two hours for 48 h. As shown in Fig. 2D, the ICG signal of B420 pellets dissipated by 12 h of culture. This is further verified by fluorescence of the ICG-B420 culture supernatant (Fig. 2E).

Because loss of the ICG-B420 signal (12 h) *in vitro* was within the time frame of murine gut transit time (8 h), we wished to determine if the ICG-B420 signal persisted as B420 traveled through the GI tract. We administered by gavage either B420 (10^9CFU/ml), ICG (0.01 mg/ml), or ICG-labeled B420 (0.01 mg/ml ICG in culture media) in 500 ul of saline. Mice from each experimental group were anesthetized at a range of timepoints (15 mins-8 h post gavage) and imaged for ICG-B420 (bio) fluorescence. The ICG-B420 signal was observable in the intact animal *in vivo* (Fig. 3A–C). Relative intensities of the ICG-B420 signal was not different between specific regions along the GI tract (Fig. 3D).

Next, mice were sacrificed at each timepoint and the GI tracts were dissected for fluorescence imaging. As shown in Fig. 3E, there is no

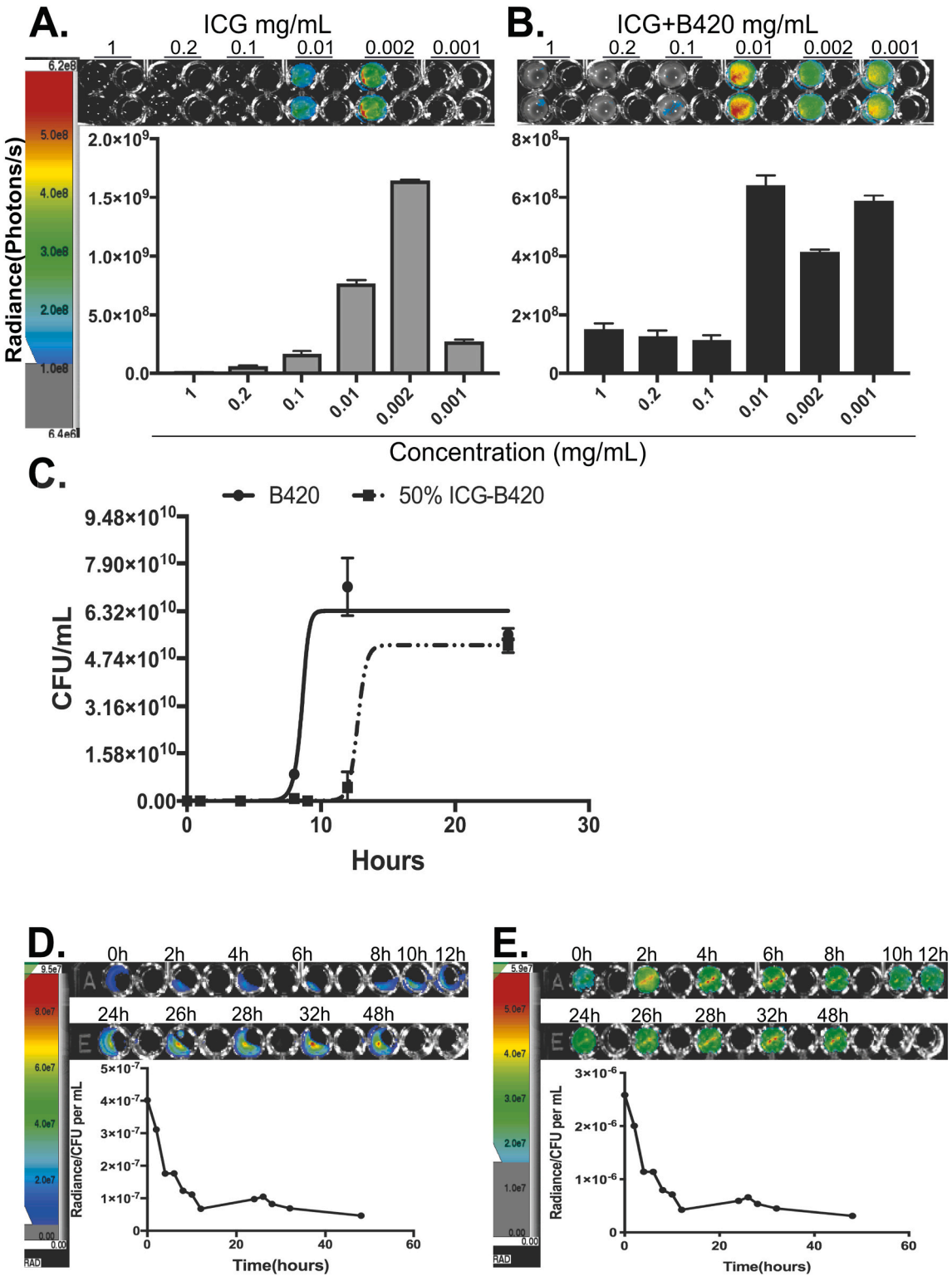

Fig. 2. Visualization of ICG-labeled B420 *in vitro*. A: ICG solution at different concentrations (0.0001–1 mg/ml) imaged in a 96 well plate (top panel) and quantified (bottom panel) as Radiance (Photons/Sec) (gray bars) ($n = 2$). B: B420 cultures (10^9 CFU/ml) incubated at different ICG concentrations (0.0001–1 mg/ml) imaged in a 96 well plate (top panel) and quantified (bottom panel) as Radiance (Photons/Sec) (black bars) (n = 2). C: Asymmetric sigmoidal growth curves of B420 alone (solid) or and ICG-B420 (dashed) (n = 2). D: Pellets of ICG-B420 co-cultures imaged every 2 h over a 48-h period in a 96 well plate (top panel) and quantified (bottom panel) as Radiance (Photons/Sec). E: Supernatant (1 ml) from ICG-B420 co-culture pellets imaged every 2 h over a 48-h period in a 96 well plate (top panel) and quantified (bottom panel) as Radiance (Photons/Sec) normalized to CFU/ml) (n = 2).

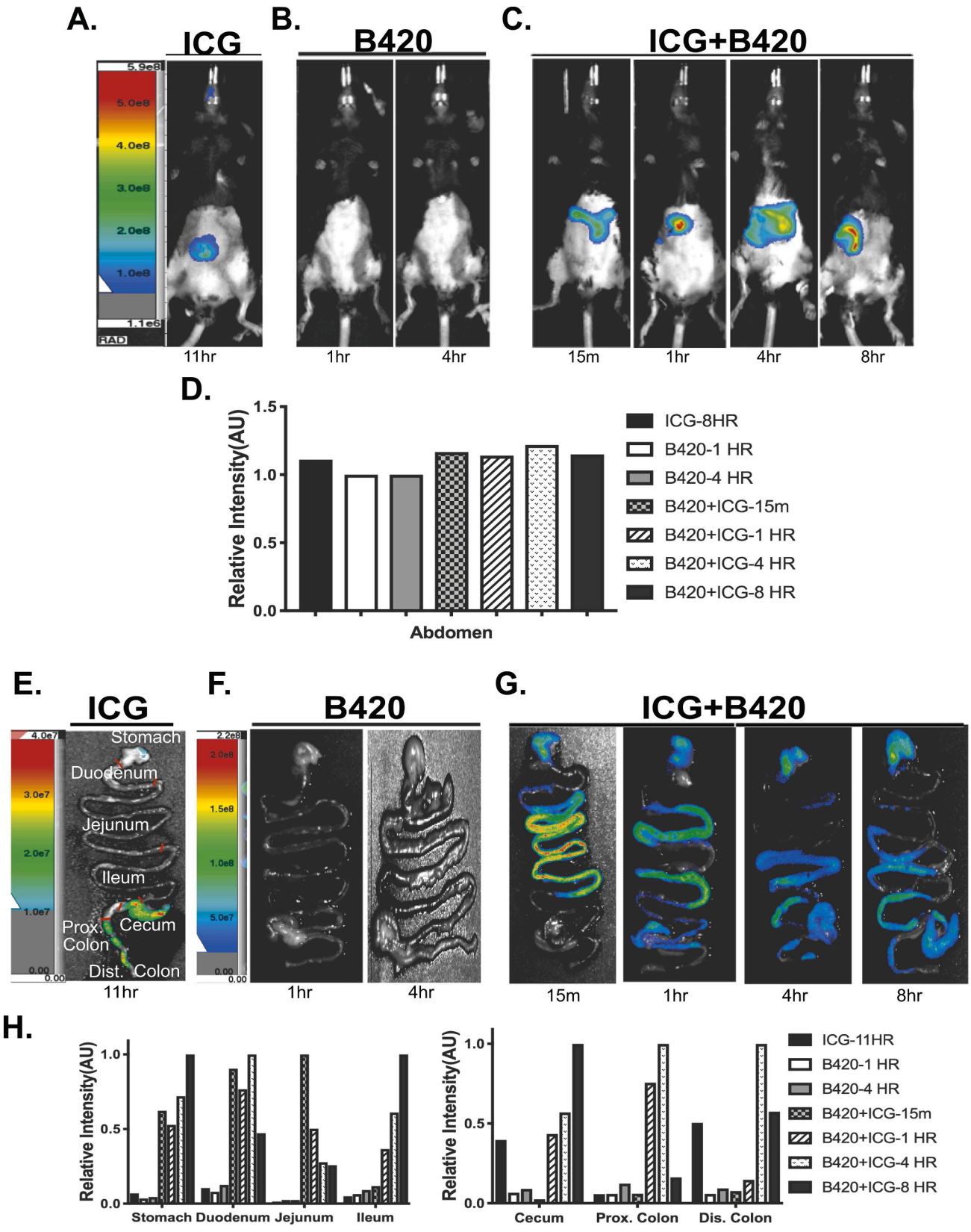

Fig. 3. Visualization of ICG-labeled B420 in vivo and ex vivo. A–C: (Bio) flourescent images (LAGOX instrument and AMIVIEW software package) of mice receiving 0.5 ml by gavage of either ICG-Saline (1.0 mg/ml), B420 (109CFU/ml) or B420 culture (10^9CFU/ml) incubated with ICG (0.01 mg/ml) ($n = 1$). D: Bar graph representation of (bio) flourescent relative intensity (AU, arbitrary units) of mouse abdomen at each time period (n = 1). E–G: (Bio) flourescent images (LAGOX instrument and AMIVIEW software package) of excised mouse GI tract after receiving 0.5 ml by gavage of either ICG-Saline (1.0 mg/ml), B420 (10^9CFU/ml) or B420 culture (10^9CFU/ml) incubated with ICG (0.01 mg/ml) (n = 1). H: Bar graph representation of (bio) flourescent relative intensity (AU, arbitrary units) of excised mouse GI tract at each time period (n = 2).

residual fluorescence along the GI tract following delivery of ICG alone in saline. Similarly, B420 harbors no fluorescence at any section of the GI tract (Fig. 3F). When B420 cultured with ICG was administered to mice by gavage, ICG fluorescence was detectable at regions along the GI tract that correlated with the specific timepoint of sacrifice (Fig. 3G). The intensity of the ICG-B420 fluorescence signal was also measured from each region of the GI tract, and the relative intensity was displayed in bar graph form (Fig. 3H). Within the first 15 min after gavage, the ICG-B420 signal was detectable in the stomach and upper intestine including the duodenum, jejunum, and ileum. The ICG-B420 fluorescence gradually translocated to the cecum, proximal and distal colon at 4- and 8-h following gavage. At the 4 and 8-h timepoint, the ICG-B420 signal was prominent in the distal portions of small intestine, cecum and colon, yet remained visible in the stomach and upper intestine, although to a lesser extent compared to the 15-min timepoint.

3.2. Genomic tracking of B420 in the GI tract

The values obtained from the ICG-B420 fluorescence provided a semi-quantitative assessment of B420 localization. Using primers specific for B420 and primers targeting the V3 region of bacterial 16 s rRNA gene, we measured B420 along the GI tract at different time intervals with quantitative PCR (qPCR). First, we validated primer sets using a purified culture of B420. Amplification products were confirmed by gel electrophoresis and sequencing (Fig. S3A and B) (Stahl and Barrangou, 2012). Furthermore, both PCR and qPCR verified the purity of the B420 culture with correlation coefficients of $R^2 = 0.79$ (PCR; Fig. S3C) and $R^2 = 0.98$ (qPCR; Fig. S5B).

Next, bacterial gDNA was isolated from each of the above described regions along the GI tract. In general, the amounts of B420 measured by qPCR followed closely to the ICG-B420 fluorescence. These data are displayed in a bar graph summary where the regional distribution along GI tract is illustrated by time at 15 min, 2, 4, and 8 h (Fig. 4A) and in a line graph summary grouped by region along the GI tract (Fig. 4B). Within 15 min from the time of gavage, B420 was detectable in the ileum up to 0.1 ng of total gDNA. By two hours post-gavage, B420 translocated to the distal portion of the GI tract with the greatest amount measured in the cecum and proximal colon (0.3–0.4 ng of gDNA). At 4 h post-gavage, B420 remained detectable in the cecum, proximal and distal colon, but, by 8 h, B420 was only detectable in the distal colon. B420 presence at each of the timepoints was validated by gel electrophoresis (Fig. S4).

Loss of B420 presence as a single gavage bolus translocated to distal portions of the gut indicates a lack of detectable B420 adherence to the upper GI tract. However, transit time is relatively rapid compared to B420 proliferation doubling time (Fig. S1 growth curve), and these data do not rule out the possibility of B420 colonization of the GI tract. Our previous work demonstrated B420 efficacy to attenuate cardiac damage after at least seven days of daily B420 administration by gavage (Danilo et al., 2017). Therefore, to determine if and where B420 colonizes along the GI tract, we administered by gavage 10 consecutive days of B420 (10^{11}CFU). Mice were then sacrificed and bacterial gDNA was extracted from each region of the GI tract at 15 min, 24 h, 48 h, and 144 h after the final gavage. Gel electrophoresis validated the qPCR. Again, these data are displayed in a bar graph summary where the regional distribution along GI tract is grouped by time at 15 min, 2, 4, and 8 h (Fig. 4C) and in a line graph summary grouped by region along the GI tract (Fig. 4D). After 15 min from the final gavage bolus, the amount of B420 in the upper GI tract (duodenum, jejunum, and ileum) reached similar levels as above (up to 0.1 ng of genomic DNA). These B420 levels dropped to 0.001 ng or less of genomic DNA in all regions of the gut 24 h post-gavage. By 48 and 144 h from final gavage bolus, B420 levels were undetectable with interpolated amounts less than 0.0001 ng of genomic DNA. These data suggest B420 did not adhere nor colonize any region of the GI tract in a significant amount.

4. Discussion

Advancing potential therapeutic uses of exogenously delivered probiotic species may depend on the ability to measure the rate, location, and abundance of these species as they transit through the gut. Key findings from our study include: (1) ICG was a more effective labeling agent over ISOVUE-300 for the bacterial strain tested, B420; (2) B420 transit time matched murine gut motility, and (3) B420 did not adhere and colonize the intestinal mucosa of the host gut microbiome. Following ingestion, it is estimated that only 20%–40% live bacterial strains reach the lower intestinal tract due to a highly acidic environment (pH ~2) and unique microenvironments along the GI tract (Bezkorovainy, 2001). This number is variable, and probiotic viability may be improved by route of administration such as in food, capsules, or alternative formulations (Govender et al., 2013). Probiotic survival is also species specific. For example, commensal bacteria appear to be particularly well-suited for gut survival, as they have developed tolerance to these microenvironments, like bile acids (Bezkorovainy, 2001; Bhardwaj et al., 2010).

Apart from survival and viability, adherence and colonization potential along the GI tract are suggested as key components impacting probiotic efficacy. Probiotic strains adhere to intestinal epithelial-like Caco-2 cells *in vitro* (Bezkorovainy, 2001; Fontaine et al., 1994). Similarly, previous work shows permanent colonization in germ-free or antibiotic treated mice (Romond et al., 1997; Tannock et al., 1988). Yet, while probiotic species remain detectable in fecal samples within an administration period, detection typically falls rapidly after discontinuation of treatment (Firmesse et al., 2007; Gerritsen et al., 2011; Satokari et al., 2001) (Sanders, 2011; Smith et al., 2011). Interestingly, the probiotic, *Lactobacillus rhamnosus* GG, remains detectable in colon biopsies after presence was lost in fecal samples from humans (Alander et al., 1999). In addition to specific microenvironments and probiotic species, *in vivo* characteristics cannot be easily recapitulated in cell-culture models.

Nevertheless, pinpointing probiotic activity along the GI tract is critical for determining mechanisms of host-microbe interaction and advancing therapeutic uses for probiotics. The application of fluorescence strategies to label bacterial strains have provided unique insights into disease processes and underlying mechanisms of host-microbe interactions. In previous studies, bacterial pathogens engineered to express luciferase, an enzyme capable of generating (bio) fluorescence, allowed rapid *in vivo* localization and quantification of the specific pathogen. Using a similar technique, *Lactobacillus plantarum* and *Lactococcus lactis* were also engineered with fluorescence green or red luciferase, which allowed detection *in vivo* and *in vitro* (Daniel et al., 2015; Doyle et al., 2004). However, these standard molecular techniques are not easily reproduced in *Bifidobacterium* due to poor genetic accessibility imposing unique challenges for genetic modifications (Grimm et al., 2014).

Here, we describe an efficient, straightforward technique that allowed, for the first time, direct tracking of B420 along the GI tract without the need for genetic manipulation. Although incubation of B420 with ISOVUE, a widely utilized contrast agent, showed a time- and dose-dependency of labeling, standard x-ray fluoroscopy imaging yielded a signal with high background and poor resolution. Without adequate measurement of spatial or temporal dynamics, ISOVUE and standard x-ray fluoroscopy detection techniques limit the utility of this approach for further resolution of gut spatial mechanisms of B420-dependent effects.

Incubating B420 with ICG provided a more robust and quantifiable approach to label and track B420. Detection of a (bio) fluorescent signal *in vivo* was established early on but only in mice delivered with genetically transformed bacteria (Contag and Bachmann, 2002). While imaging the whole mouse, the ICG-B420 signal was observed in the abdomen. However, *in vivo* localization of the ICG-B420 signal was indistinguishable over time due to the overlapping and tortuous anatomy of the intestinal tract. Although this finding is not unique to our

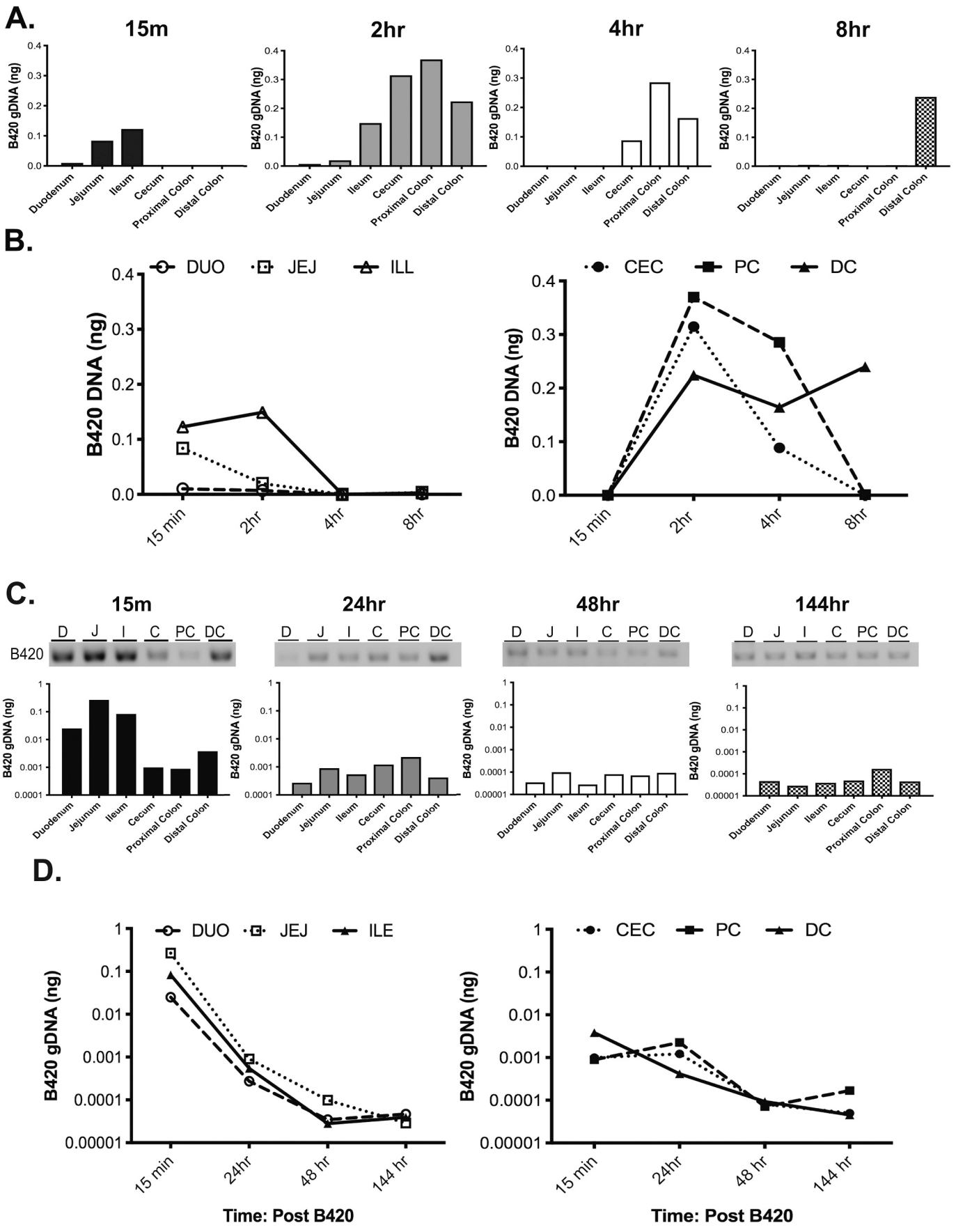

(caption on next page)

Fig. 4. Genomic tracking of B420 in the GI tract. A: Bar graph representation of B420 genomic DNA (gDNA) extracted from mouse GI tract following 0.5 ml of B420 (10^9CFU/ml) by gavage and quantified by qPCR (see Methods and Supplemental Figs. S2–3) along identified regions and 15 m, 2 h, 4 h and 8 h. B: Line graph representation derived from same samples as A showing time course of B420 gDNA extracted from mouse GI tract following 0.5 ml of B420 (10^9CFU/ml) by gavage and quantified by qPCR at upper duodenum (DUO; dashed open circle), jejunum (JEJ; dashed open square), ileum (ILL; solid line open triangle) cecum (CEC; dashed filled circle), proximal colon (PC; dashed filled square) and distal colon (DC; solid line filled triangle) (n = 1). C: Agarose gel images (top panel) and bar graph representation (bottom panel) of PCR products following amplification of B420 gDNA extracted from mouse GI tract following 0.5 ml of B420 (10^9 CFU/ml) by gavage and quantified by qPCR (see Methods and Supplemental Figs. S2–3) along identified regions and 15 m, 24 h, 48 h and 144 h starting at the end of 10 consecutive days of administration. D: Line graph representation derived from same samples in C showing time course of B420 gDNA extracted from mouse GI tract following 0.5 ml of B420 (10^9CFU/ml) by gavage and quantified by qPCR at upper duodenum (DUO; dashed open circle), jejunum (JEJ; dashed open square), ileum (ILL; solid line open triangle) cecum (CEC; dashed filled circle), proximal colon (PC; dashed filled square) and distal colon (DC; solid line filled triangle) (n = 1).

study, it restricts precise determination of B420 localization and/or potential colonization in the intact mouse (Daniel et al., 2015; Wiles et al., 2006). Conversely, imaging excised GI tract at different time intervals following delivery of ICG-B420 resulted in localized fluorescence at distinct regions along the GI tract. Fluorescence of the ICG-B420 signal paralleled murine gut transit time, where a single bolus administration quickly passed the upper intestinal tract and reached the distal colon and cecum within 8 h. We validated the ICG-B420 signal using qPCR; qPCR of B420 matched the fluorescence in addition to providing a quantitative assessment of B420 and commensal bacteria amounts.

Given the observed transit of B420 following a single administration, we investigated how 10 consecutive days of treatment would impact B420 localization, adhesion, and residence along the GI tract. Following 10 days of daily B420 delivery, the time course of ICG-B420 signal following the final bolus mirrored B420 transit after a single bolus in a naïve, untreated mouse. This suggested that B420 does not adhere and colonize to the intestinal mucosa even with extended delivery of B420. This finding was surprising because previous work showed B420 and other *Bifidobacterium* strains demonstrate mucosal adherence in isolated preparations from infants and adults using an *in vitro* adhesion assay (Ouwehand et al., 1999).

Despite no measurable mucosal colonization, it is possible that B420 colonization becomes compromised as it transits across the GI tract. However, the recovery rate of a *Bifidobacterium* strain in human stool samples was reported to be near 30% of the ingested dose (Bouhnik et al., 1992), which is similar to the percentage of probiotic that survives passage through the stomach (Bezkorovainy, 2001). Furthermore, other studies report probiotic persistence up to a week after ceasing probiotic ingestion (Alander et al., 1999; Bouhnik et al., 1992; Gerritsen et al., 2011).

In general, very few exogenous microorganisms including pathogens can establish residency in the gut, unless the gut is compromised (*i.e. via* antibiotics or dysbiosis), even though the cecal microenvironment is ideal for bacterial colonization, growth, and adherence (Gu et al., 2013; Nguyen et al., 2015). This "colonization resistance" is well-recognized and is a direct result of the diversity and sheer volume of bacterial species within the gut limiting available space for non-native bacterial species. Commensal species also generate inhibitory metabolites and create nutrient "niches," establishing a competitive environment for any non-commensal bacteria to inhabit (Pickard et al., 2017; Rajilić-Stojanović et al., 2007). Consequently, *in-vitro* adherence assays cannot replicate competitive interactions among bacterial species that exists in the host microbiome of the GI tract (Chauviere et al., 2009; Said et al., 2014; Turroni et al., 2013).

An important step towards acceptance of this approach is providing direct relevance towards disease states. The anti-obesity potential of B420 is well-documented in both rodent models of obesity and human clinical trials (Amar et al., 2011; Hibberd et al., 2019; Stenman et al., 2014b). Accumulating evidence suggests that B420 administration interacts with the gut epithelium and modifies commensal bacteria to strengthen barrier integrity, dampen inflammation, and improve glucose tolerance which are often disrupted in the dysbiotic gut. We recently ascribed a fundamental role of B420 and the gut to protecting against myocardial ischemic injury (Danilo et al., 2017). As part of these studies, supplementation for as little as seven days with B420 protects the heart against ischemic damage (Danilo et al., 2017). Considering the requirement for seven days and loss of B420 presence by six days (144 h), we tested whether intermittent delivery for five consecutive days separated by five days of saline would attenuate weight gain and/or cardiac damage. The implicit suggestion is that continued delivery of B420 is required to impart a physiological benefit. Furthermore, B420 may act similar to a pharmaceutical where dosing titration is required to maximize benefit. However, we show that intermittent delivery of B420 alternating every five days did not protect against weight gain or cardiac injury demonstrated previously following persistent, daily delivery of B420 (**Fig. S8**).

4.1. Implications, limitations and future directions

The gut is the largest organ system in the body involved in immunological regulation and is highly influenced resident flora. The gut microbiota comprises the gut microbiome and are necessary for maintaining immune health. Alterations between mutualistic interactions of the host's immune system with colonic microbiota metabolites and antigens initiate and perpetuate uncontrolled inflammation in the intestinal mucosa and in some cases potentiate metabolic and inflammatory disorders including obesity, diabetes, and cardiovascular disease. A possible approach to treat these disorders involves modulating the gut microbiome through the administration of probiotics. Understanding the mechanism through which gut health affects these disorders will allow for more targeted and effective treatment options. The aim of our research is to identify localization of the probiotics to better understand potential initiation sites of a novel anti-inflammatory cascade that attenuates the extent of heart disease.

Clear evidence exists that probiotics can shift microbial populations or "correct" a dysbiotic gut (McFarland, 2014). The implication from this study suggests ICG may be exploited to track probiotic species in the gut. The long-term implication is that B420 colonization of the host microbiome by B420, and perhaps alternative probiotic species, is not necessary to impart a cardioprotective or weight gain effect. Having a beneficial impact on host health without colonization is not necessarily unique to B420. Other, well-studied probiotic strains such as *Lactobacillus rhamnosus* GG and Bifidobacterium lactis B12, have demonstrated similar functionality without establishing residency within the host (Salminen and Isolauri, 2006). Interestingly, introduction of Bifidobacterium to the infant gut through breast feeding promotes microbiota development and persists within the GI tract indefinitely (Guarner and Malagelada, 2003).

An important limitation of our study is the use of mice with a "normal", non-disrupted microbiome. It is possible that B420 delivery into a dysbiotic gut may establish residency or demonstrate a unique adherence pattern. Furthermore, colonization and adherence may be strain-dependent. Future work will be directed at regional elucidation of B420 mechanism and inclusion of multiple strain combinations into the study design as well as determination of soluble or other factors expressed during gut transit that may further drive microbiome-mediated protective effects.

Declaration of Competing Interest

The authors declare that they have no known competing financial interests or personal relationships that could have appeared to influence the work reported in this paper.

Acknowledgements

This work was supported by the National Institutes of Health (NIH) grant HL098256, the American Heart Association (AHA) grant 16GRNT31390006, and independent and interdisciplinary trainings in biomedical engineering and cardiovascular sciences (5T32HL00795515, 5T32 HL007249, and T32 GM132008). Support was also received from the University of Arizona Sarver Heart Center.

Appendix A. Supplementary data

Supplementary data to this article can be found online at https://doi.org/10.1016/j.mimet.2021.106302.

References

Alander, M., Satokari, R., Korpela, R., Vilpponen-salmela, T., Mattila-sandholm, T., Von Wright, A., 1999. Persistence of colonization of human colonic mucosa by a probiotic strain, *Lactobacillus rhamnosus* GG, after oral consumption persistence of colonization of human colonic mucosa by a probiotic strain, *Lactobacillus rhamnosus* GG, after oral consumption. Appl. Environ. Microbiol. 65, 351–354.

Alander, J.T., Kaartinen, I., Laakso, A., Pätilä, T., Spillmann, T., Tuchin, V.V., Venermo, M., Välisuo, P., 2012. A review of indocyanine green fluorescent imaging in surgery. Int. J. Biomed. Imaging 2012, 1–26. https://doi.org/10.1155/2012/940585.

Amar, J., Chabo, C., Waget, A., Klopp, P., Vachoux, C., Bermúdez-Humarán, L.G., Smirnova, N., Bergé, M., Sulpice, T., Lahtinen, S., Ouwehand, A., Langella, P., Rautonen, N., Sansonetti, P.J., Burcelin, R., 2011. Intestinal mucosal adherence and translocation of commensal bacteria at the early onset of type 2 diabetes: molecular mechanisms and probiotic treatment. EMBO Mol. Med. https://doi.org/10.1002/emmm.201100159.

Bauer, P., Duca, F.A., Waise, T.M.Z., Dranse, H.J., Rasmussen, B.A., Puri, A., Rasti, M., O'Brien, C.A., Lam, T.K.T., 2018a. Lactobacillus gasseri in the upper small intestine impacts an ACSL3-dependent fatty acid-sensing pathway regulating Whole-Body Glucose Homeostasis. Cell Metabol. 27, 572–587. https://doi.org/10.1016/j.cmet.2018.01.013, 29514066.

Bauer, P.V., Duca, F.A., Waise, T.M.Z., Rasmussen, B.A., Abraham, M.A., Dranse, H.J., Puri, A., O'Brien, C.A., Lam, T.K.T., 2018b. Metformin Alters Upper Small Intestinal Microbiota that Impact a Glucose-SGLT1-Sensing Glucoregulatory Pathway. Cell Metab. 27, 101–117. https://doi.org/10.1016/j.cmet.2017.09.019, 29056513.

Bezkorovainy, A., 2001. Probiotics: determinants of survival and growth in the gut. Am. J. Clin. Nutr. 73, 399–405.

Bhardwaj, A., Gupta, H., Kapila, S., Kaur, G., Vij, S., Malik, R.K., 2010. Safety assessment and evaluation of probiotic potential of bacteriocinogenic enterococcus faecium KH 24 strain under in vitro and in vivo conditions. Int. J. Food Microbiol. 141, 156–164. https://doi.org/10.1016/j.ijfoodmicro.2010.05.001.

Bouhnik, Y., Pochart, P., Marteau, P., Arlet, G., Goderel, I., Rambaud, J.C., 1992. Fecal recovery in humans of viable Bifidobacterium sp ingested in fermented milk. Gastroenterology. https://doi.org/10.1016/0016-5085(92)90172-U.

Brown, E.M., Sadarangani, M., Finlay, B.B., 2013. The role of the immune system in governing host-microbe interactions in the intestine. Nat. Immunol. 14, 660–667. https://doi.org/10.1038/ni.2611, 23778793.

Chauviere, G., Coconnier, M.-H., Kerneis, S., Fourniat, J., Servin, A.L., 2009. Adhesion of human Lactobacillus acidophilus strain LB to human enterocyte-like Caco-2 cells. J. Gen. Microbiol. 138, 1689–1696. https://doi.org/10.1099/00221287-138-8-1689.

Contag, C.H., Bachmann, M.H., 2002. Advances in in vivo bioluminescence imaging of gene expression. Annu. Rev. Biomed. Eng. https://doi.org/10.1146/annurev.bioeng.4.111901.093336.

Daniel, C., Poiret, S., Dennin, V., Boutillier, D., Lacorre, D.A., Foligné, B., Pot, B., 2015. Dual-color bioluminescence imaging for simultaneous monitoring of the intestinal persistence of lactobacillus plantarum and Lactococcus lactis in living mice. Appl. Environ. Microbiol. 81, 5344–5349. https://doi.org/10.1128/aem.01042-15.

Danilo, C.A., Constantopoulos, E., McKee, L.A., Chen, H., Regan, J.A., Lipovka, Y., Lahtinen, S., Stenman, L.K., Nguyen, T.V.V., Doyle, K.P., Slepian, M.J., Khalpey, Z.I., Konhilas, J.P., 2017. Bifidobacterium animalis subsp. lactis 420 mitigates the pathological impact of myocardial infarction in the mouse. Benef. Microbes 8, 257–269. https://doi.org/10.3920/BM2016.0119.

Derrien, M., van Passel, M.W.J., van de Bovenkamp, J.H.B., Schipper, R.G., de Vos, W.M., Dekker, J., 2010. Mucin-bacterial interactions in the human oral cavity and digestive tract. Gut Microbes 1, 254–268. https://doi.org/10.4161/gmic.1.4.12778, 21327032.

DeSesso, J.M., Jacobson, C.F., 2001. Anatomical and physiological parameters affecting gastrointestinal absorption in humans and rats. Food Chem. Toxicol. 39, 209–228. https://doi.org/10.1016/s0278-6915(00)00136-8, 11278053.

Dominguez, W., O'Sullivan, D.J., 2013. Developing an efficient and reproducible conjugation-based gene transfer system for bifidobacteria. Microbiol. 159, 328–338. https://doi.org/10.1099/mic.0.061408-0, 23197173.

Donaldson, G.P., Lee, S.M., Mazmanian, S.K., 2015. Gut biogeography of the bacterial microbiota. Nat. Rev. Microbiol. 14, 20–32. https://doi.org/10.1038/nrmicro3552, 26499895.

Doyle, T.C., Burns, S.M., Contag, C.H., 2004. In vivo bioluminescence imaging for integrated studies of infection. Cell. Microbiol. 6, 303–317. https://doi.org/10.1111/j.1462-5822.2004.00378.x.

Fang, H., Gough, J., 2013. DcGO: Database of domain-centric ontologies on functions, phenotypes, diseases and more. Nucleic Acids Res. 41, 536–544. https://doi.org/10.1093/nar/gks1080, 23161684.

Firmesse, O., Mogenet, A., Bresson, J.L., Corthier, G., Furet, J.P., 2007. Lactobacillus rhamnosus R11 consumed in a food supplement survived human digestive transit without modifying microbiota equilibrium as assessed by real-time polymerase chain reaction. J. Mol. Microbiol. Biotechnol. 14, 90–99. https://doi.org/10.1159/000106087.

Fontaine, I.F., Aissi, E.A., Bouquelet, S.J.L., 1994. In vitro binding of Bifidobacterium bifidum DSM 20082 to mucosal glycoproteins and hemagglutinating activity. Curr. Microbiol. 28, 325–330. https://doi.org/10.1007/BF01570196.

Gale, J.S., Proulx, A.A., Gonder, J.R., Mao, A.J., Hutnik, C.M.L., 2004. Comparison of the in vitro toxicity of indocyanine green to that of trypan blue in human retinal pigment epithelium cell cultures. Am J. Ophthalmol. https://doi.org/10.1016/j.ajo.2004.02.061.

Gerritsen, J., Smidt, H., Rijkers, G.T., De Vos, W.M., 2011. Intestinal microbiota in human health and disease: the impact of probiotics. Genes Nutr. 6, 209–240. https://doi.org/10.1007/s12263-011-0229-7.

Giraldo, J., Vivas, N.M., Vila, E., Badia, A., 2002. Assessing the (a)symmetry of concentration-effect curves. Pharmacol. Ther. 95, 21–45. https://doi.org/10.1016/s0163-7258(02)00223-1, 12163126.

Gottschalk, P.G., Dunn, J.R., 2005. The five-parameter logistic: a characterization and comparison with the four-parameter logistic. Anal. Biochem. 343, 54–65. https://doi.org/10.1016/j.ab.2005.04.035, 15953581.

Govender, M., Choonara, Y.E., Kumar, P., du Toit, L.C., van Vuuren, S., Pillay, V., 2013. A review of the advancements in probiotic delivery: conventional vs. non-conventional formulations for intestinal Flora supplementation. AAPS PharmSciTech 15, 29–43. https://doi.org/10.1208/s12249-013-0027-1.

Grimm, V., Gleinser, M., Neu, C., Zhurina, D., Riedel, C.U., 2014. Expression of fluorescent proteins in bifidobacteria for analysis of host-microbe interactions. Appl. Environ. Microbiol. 80, 2842–2850. https://doi.org/10.1128/AEM.04261-13.

Grisanti, S., Szurman, P., Gelisken, F., Aisenbrey, S., Oficjalska-Mlynczak, J., Bartz-Schmidt, K.U., 2004. Histological findings in experimental macular surgery with indocyanine green. Investig. Ophthalmol. Vis. Sci. https://doi.org/10.1167/iovs.03-0797.

Gu, S., Chen, D., Zhang, J.N., Lv, X., Wang, K., Duan, L.P., Nie, Y., Wu, X.L., 2013. Bacterial community mapping of the mouse gastrointestinal tract. PLoS One 8. https://doi.org/10.1371/journal.pone.0074957.

Guarner, F., Malagelada, J.R., 2003. Gut flora in health and disease. Lancet. https://doi.org/10.1016/S0140-6736(03)12489-0.

Hibberd, A.A., Yde, C.C., Ziegler, M.L., Honoré, A.H., Saarinen, M.T., Lahtinen, S., Stahl, B., Jensen, H.M., Stenman, L.K., 2019. Probiotic or synbiotic alters the gut microbiota and metabolism in a randomised controlled trial of weight management in overweight adults. Benef. Microbes. https://doi.org/10.3920/BM2018.0028.

Hotamisligil, G.S., 2017. Inflammation, metaflammation and immunometabolic disorders. Nature 542, 177–185. https://doi.org/10.1038/nature21363, 28179656.

Karlsson, F., Tremaroli, V., Nielsen, J., Bäckhed, F., 2013. Assessing the human gut microbiota in metabolic diseases. Diabetes 62, 3341–3349. https://doi.org/10.2337/db13-0844, 24065795.

Lee, J.-H., O'Sullivan, D.J., 2010. Genomic insights into bifidobacteria. Microbiol. Mol. Biol. Rev. 74, 378–416. https://doi.org/10.1128/MMBR.00004-10, 20805404.

McFarland, L.V., 2014. Use of probiotics to correct dysbiosis of normal microbiota following disease or disruptive events: a systematic review. BMJ Open. https://doi.org/10.1136/bmjopen-2014-005047.

Milani, C., Duranti, S., Lugli, G.A., Bottacini, F., Strati, F., Arioli, S., Foroni, E., Turroni, F., van Sinderen, D., Ventura, M., 2013. Comparative genomics of Bifidobacterium animalis subsp. lactis reveals a strict monophyletic bifidobacterial taxon. Appl. Environ. Microbiol. 79, 4304–4315. https://doi.org/10.1128/AEM.00984-13, 23645200.

Mowat, A.M., Agace, W.W., 2014. Regional specialization within the intestinal immune system. Nat. Rev. Immunol. 667–685. https://doi.org/10.1038/nri3738, 25234148.

Nguyen, T.L.A., Vieira-Silva, S., Liston, A., Raes, J., 2015. How informative is the mouse for human gut microbiota research? Dis. Model. Mech. 8, 1–16. https://doi.org/10.1242/dmm.017400.

Ouwehand, A.C., Isolauri, E., Kirjavainen, P.V., Salminen, S.J., 1999. Adhesion of four Bifidobacterium strains to human intestinal mucus from subjects in different age groups. FEMS Microbiol. Lett. 172, 61–64. https://doi.org/10.1016/S0378-1097(99)00013-0.

Pickard, J.M., Zeng, M.Y., Caruso, R., Núñez, G., 2017. Gut microbiota: role in pathogen colonization, immune responses, and inflammatory disease. Immunol. Rev. https://doi.org/10.1111/imr.12567.

Putaala, H., Barrangou, R., Leyer, G.J., Ouwehand, A.C., Bech Hansen, E., Romero, D.A., Rautonen, N., 2010. Analysis of the human intestinal epithelial cell transcriptional response to Lactobacillus acidophilus, Lactobacillus salivarius, Bifidobacterium

lactis and Escherichia coli. Benef. Microbes 1, 283–295. https://doi.org/10.3920/BM2010.0003, 21831765.
Putaala, H., Salusjärvi, T., Nordström, M., Saarinen, M., Ouwehand, A.C., Bech Hansen, E., Rautonen, N., 2008. Effect of four probiotic strains and Escherichia coli O157:H7 on tight junction integrity and cyclo-oxygenase expression. Res. Microbiol. 159 (9–10), 692–698. https://doi.org/10.1016/j.resmic.2008.08.002, 18783733.
Rajilić-Stojanović, M., Smidt, H., De Vos, W.M., 2007. Diversity of the human gastrointestinal tract microbiota revisited. Environ. Microbiol. 9, 2125–2136. https://doi.org/10.1111/j.1462-2920.2007.01369.x.
Romond, M.B., Haddou, Z., Mielcareck, C., Romond, C., 1997. Bifidobacteria and human health: regulatory effect of indigenous bifidobacteria on *Escherichia coli* intestinal colonization. In: Anaerobe. https://doi.org/10.1006/anae.1997.0089.
Said, J., Mochizuki, K., Homma, N., 2014. Affinity of the Bifidobacterium to intestinal mucosal epithelial cells. Bifidobact. Microflora 1, 51–54. https://doi.org/10.12938/bifidus1982.1.1_51.
Salminen, S., Isolauri, E., 2006. Intestinal colonization, microbiota, and probiotics. J. Pediatr. 149, 115–120. https://doi.org/10.1016/j.jpeds.2006.06.062.
Sanders, M.E., 2011. Impact of probiotics on colonizing microbiota of the gut. J. Clin. Gastroenterol. 45, 115–119. https://doi.org/10.1097/MCG.0b013e318227414a.
Satokari, R.M., Vaughan, E.E., Akkermans, A.D.L., Saarela, M., De Vos, W.M., 2001. Polymerase chain reaction and denaturing gradient gel electrophoresis monitoring of fecal bifidobacterium populations in a prebiotic and probiotic feeding trial. VTT Publ. 231, 85–89.
Smith, T.J., Anderson, D., Margolis, L.M., Sikes, A., Young, A.J., 2011. Persistence of Lactobacillus reuteri DSM17938 in the human intestinal tract: response to consecutive and alternate-day supplementation. J. Am. Coll. Nutr. 30, 259–264. https://doi.org/10.1080/07315724.2011.10719968.
Stahl, B., Barrangou, R., 2012. Complete genome sequences of probiotic strains Bifidobacterium animalis subsp. lactis B420 and Bi-07. J. Bacteriol. https://doi.org/10.1128/JB.00766-12.
Stearns, J.C., Lynch, M.D.J., Senadheera, D.B., Tenenbaum, H.C., Goldberg, M.B., Cvitkovitch, D.G., Croitoru, K., Moreno-Hagelsieb, G., Neufeld, J.D., 2011. Bacterial biogeography of the human digestive tract. Sci. Rep. 1, 1–9. https://doi.org/10.1038/srep00170, 22355685.
Stenman, L.K., Lehtinen, M.J., Meland, N., Christensen, J.E., Yeung, N., Saarinen, M.T., Courtney, M., Burcelin, R., Lähdeaho, M.L., Linros, J., Apter, D., Scheinin, M., Kloster Smerud, H., Rissanen, A., Lahtinen, S., 2016. Probiotic with or without fiber controls body fat mass, associated with serum zonulin, in overweight and obese Adults-Randomized Controlled Trial. EBioMedicine 13, 190–200. https://doi.org/10.1016/j.ebiom.2016.10.036, 27810310.
Stenman, L.K., Waget, A., Garret, C., Klopp, P., Burcelin, R., Lahtinen, S., 2014a. Potential probiotic Bifidobacterium animalis ssp. lactis 420 prevents weight gain and glucose intolerance in diet-induced obese mice. Benef. Microbes 5, 437–445. https://doi.org/10.3920/BM2014.0014.
Stenman, L.K., Waget, A., Garret, C., Klopp, P., Burcelin, R., Lahtinen, S., 2014b. Potential probiotic Bifidobacterium animalis ssp. lactis 420 prevents weight gain and glucose intolerance in diet-induced obese mice. Benef. Microbes. https://doi.org/10.3920/BM2014.0014.
Sundquist, A., Bigdeli, S., Jalili, R., Druzin, M.L., Waller, S., Pullen, K.M., El-Sayed, Y.Y., Taslimi, M.M., Batzoglou, S., Ronaghi, M., 2007. Bacterial flora-typing with targeted, chip-based Pyrosequencing. BMC Microbiol. 7, 1–11. https://doi.org/10.1186/1471-2180-7-108, 18047683.
Tannock, G.W., Crichton, C., Welling, G.W., Koopman, J.P., Midtvedt, T., 1988. Reconstitution of the gastrointestinal microflora of lactobacillus-free mice. Appl. Environ. Microbiol. 54, 2971–2975.
Tremaroli, V., Bäckhed, F., 2012. Functional interactions between the gut microbiota and host metabolism. Nature 489, 242–249. https://doi.org/10.1038/nature11552, 22972297.
Turroni, F., Serafini, F., Foroni, E., Duranti, S., O'Connell Motherway, M., Taverniti, V., Mangifesta, M., Milani, C., Viappiani, A., Roversi, T., Sanchez, B., Santoni, A., Gioiosa, L., Ferrarini, A., Delledonne, M., Margolles, A., Piazza, L., Palanza, P., Bolchi, A., Guglielmetti, S., van Sinderen, D., Ventura, M., 2013. Role of sortase-dependent pili of Bifidobacterium bifidum PRL2010 in modulating bacterium-host interactions. Proc. Natl. Acad. Sci. 110, 11151–11156. https://doi.org/10.1073/pnas.1303897110.
Wiles, S., Pickard, K.M., Peng, K., MacDonald, T.T., Frankel, G., 2006. In vivo bioluminescence imaging of the murine pathogen Citrobacter rodentium. Infect. Immun. 74, 5391–5396. https://doi.org/10.1128/IAI.00848-06.
Wosse, C.R., Fox, G.E., Pechman, K.R., 1977. Comparative cataloging of 16S ribosomal ribonucleic acid: molecular approach to procaryotic systematics. Int. J. Syst. Evol. Microbiol. 27 (1), 44–57. https://doi.org/10.1099/00207713-27-1-44.
Yu, Z., Morrison, M., 2004. Improved extraction of PCR-quality community DNA from digesta and fecal samples. Biotechniques 36, 808–812. https://doi.org/10.2144/04365ST04.
Zadeh-Tahmasebi, M., Duca, F.A., Rasmussen, B.A., Bauer, P.V., Côté, C.D., Filippi, B.M., Lam, T.K.T., 2016. Activation of short and long chain fatty acid sensing machinery in the ileum lowers glucose production in vivo. J. Biol. Chem. 291, 8816–8824. https://doi.org/10.1074/jbc.M116.718460, 26896795.
Zoetendal, E.G., Raes, J., Van Den Bogert, B., Arumugam, M., Booijink, C.C., Troost, F.J., Bork, P., Wels, M., De Vos, W.M., Kleerebezem, M., 2012. The human small intestinal microbiota is driven by rapid uptake and conversion of simple carbohydrates. ISME J. 6, 1415–1426. https://doi.org/10.1038/ismej.2011.212, 22258098.